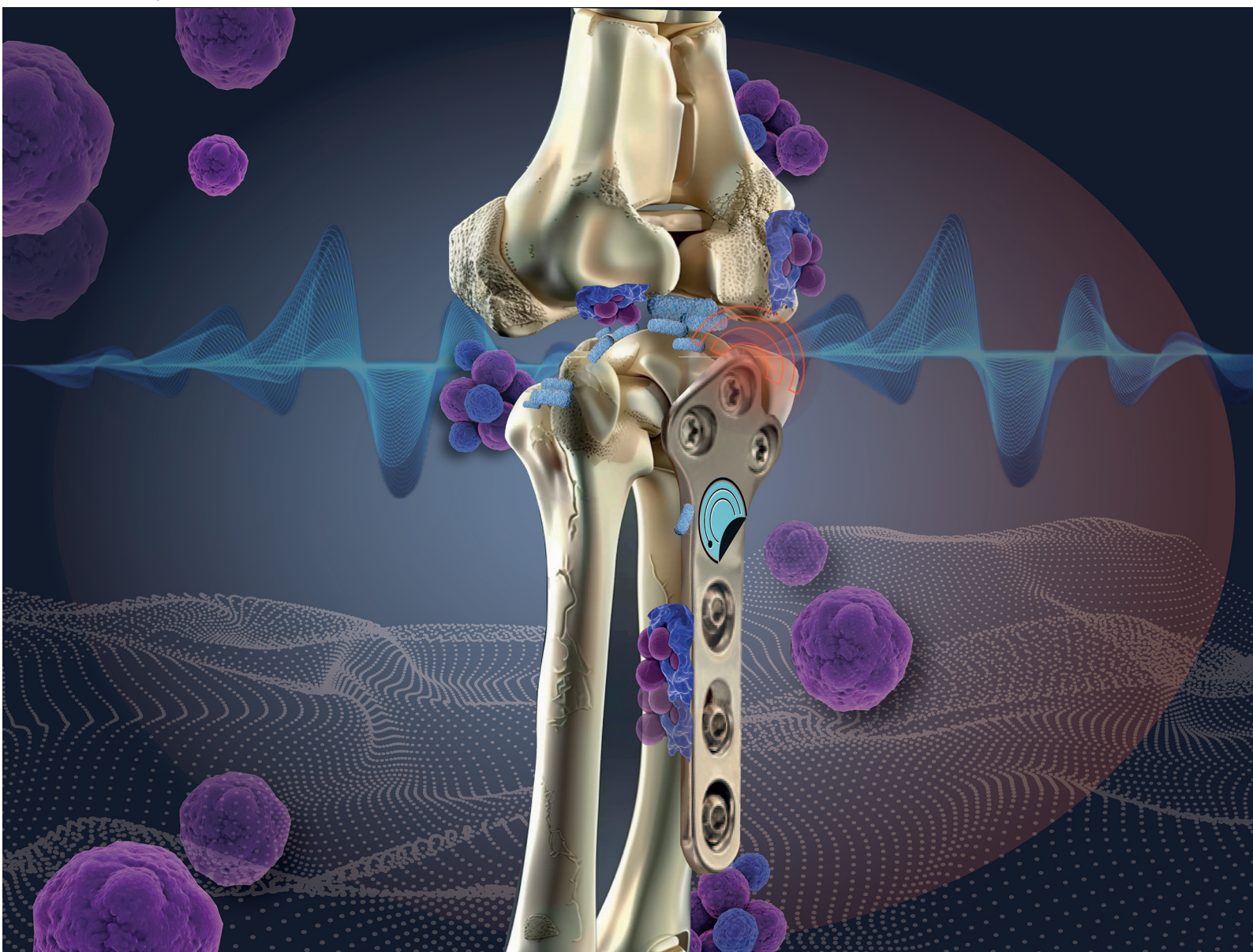


# Analyst

rsc.li/analyst




ISSN 0003-2654

**PAPER**

Fabiana Arduini *et al.*  
Functionalized orthopaedic implant as pH electrochemical  
sensing tool for smart diagnosis of hardware infection


 Cite this: *Analyst*, 2024, **149**, 3085

## Functionalized orthopaedic implant as pH electrochemical sensing tool for smart diagnosis of hardware infection†

 Luca Fiore,<sup>a,b</sup> Vincenzo Mazzaracchio,<sup>a</sup> Christian Gosti,<sup>a</sup> Leonardo Duranti,<sup>a</sup> Raffaele Vitiello,<sup>c,d</sup> Giulio Maccauro<sup>c,d</sup> and Fabiana Arduini  <sup>\*a,b</sup>

In the orthopaedic surgery field, the use of medical implants to treat a patient's bone fracture is nowadays a common practice, nevertheless, it is associated with possible cases of infection. The consequent hardware infection can lead to implant failure and systemic infections, with prolonged hospitalization, time-consuming rehabilitation treatments, and extended antibiotic therapy. Hardware infections are strictly related to bacterial adhesion to the implant, leading to infection occurrence and consequent pH decreasing from physiological level to acid pH. Here, we demonstrate the new strategy to use an orthopaedic implant functionalized with iridium oxide film as the working electrode for the potentiometric monitoring of pH in hardware infection diagnosis. A functional investigation was focused on selecting the implant material, namely titanium, titanium alloy, and stainless steel, and the component, namely screws and implants. After selecting the titanium-based implant as the working electrode and a silver wire as the reference electrode in the final configuration of the smart sensing orthopaedic implant, a calibration curve was performed in standard solutions. An equation equal to  $y = (0.76 \pm 0.02) - (0.068 \pm 0.002) x$ ,  $R^2 = 0.996$ , was obtained in the pH range of 4–8. Subsequently, hysteresis, interference, matrix effect, recovery study, and storage stability were investigated to test the overall performance of the sensing device, demonstrating the tremendous potential of electrochemical sensors to deliver the next generation of smart orthopaedic implants.

 Received 16th February 2024,  
 Accepted 27th April 2024

DOI: 10.1039/d4an00253a

[rsc.li/analyst](https://rsc.li/analyst)

## Introduction

The risk of infection with antibiotic resistance is an ongoing relevant issue highlighted at worldwide level, as recently reported by the European Commission.<sup>1</sup> In orthopaedic surgery, the problem of infection can be considered universal for all implanted orthopaedic devices.<sup>2</sup> Indeed, hardware infection (HI), such as in the case of using plates, screws and nails, represents one of the most devastating complications of orthopaedic surgery leading to the failure of the periprosthetic implant and, in the most serious cases, causing a systemic infection that can risk the life of the patient. HI occurs worldwide in 5% of clean orthopaedic surgery,<sup>3</sup> and it is considered to be one of the most costly infectious diseases to treat, consid-

ering that its treatment requires at least one surgery, prolonged hospitalization, rehabilitation care, prolonged antibiotic therapy, and extended absence from work in working-age patients. For instance, the economic burden associated with one HI is estimated at approximately \$51 000.<sup>4</sup> It is worthy of note that the global cost of Prosthetic Joint Infection (PJI) and HI will increase year by year, considering the need for joint arthroplasty and trauma surgery owing to the population's demographic ageing. In this regard, in the USA, the annual cost to hospitals of revision surgery for infection increased from \$320 million (€295 million) in 2001 to \$566 million (€522 million) in 2009.<sup>5</sup> In addition, PJI is a relevant translational issue in healthcare, having a highly severe social and clinical impact beyond the economic burden.<sup>6</sup> For example, in 2022, Walter *et al.* carried out a qualitative analysis of nursing staff's experiences in PJI management, highlighting that PJI has a high emotional burden for the patients, owing to the lack of social interaction contributing to it.<sup>7</sup> The difficulty of HI and PJI is mainly ascribed to difficulty in the timely correct diagnosis. The unmet medical and societal need is very well addressed in a review<sup>8</sup> written by several scientists belonging to AO Research Institute Davos, Switzerland, University Hospital of Basel, Switzerland, Ghent University, Belgium, University Hospitals Leuven, Belgium, Trauma Centre,

<sup>a</sup>Department of Chemical Science and Technologies, University of Rome "Tor Vergata", via della Ricerca Scientifica, 00133 Rome, Italy.

E-mail: [Fabiana.arduini@uniroma2.it](mailto:Fabiana.arduini@uniroma2.it)

<sup>b</sup>SENSEAMED, Via Bitonto 139, 00133 Rome, Italy

<sup>c</sup>Università Cattolica del Sacro Cuore, Rome, Italy

<sup>d</sup>Fondazione Policlinico Universitario Agostino Gemelli Istituto di Ricovero e Cura a Carattere Scientifico (IRCCS), Rome, Italy

† Electronic supplementary information (ESI) available. See DOI: <https://doi.org/10.1039/d4an00253a>

Murnau, Germany, University of Rochester Medical Center, New York, USA, MC, University of Amsterdam, The Netherlands, Virginia Commonwealth University, Virginia, USA that reported, "A considerable number of infections are 'culture-negative' despite being clinically apparent. [...] This raises the question: can we do better with diagnosis? Establishing the correct diagnosis with a new test would represent a major breakthrough in the field". Currently, hip and knee PJI are diagnosed according to the 2018 Philadelphia International Consensus Meeting. Briefly, major criteria are considered: two positive cultures or a sinus tract presence. However, in the absence of major criteria, minor criteria are considered as follows: 2 points for a serum CRP > 1 mg dL<sup>-1</sup>; 2 points for D-dimer > 860 ng mL<sup>-1</sup>; 1 point for erythrocyte sedimentation rate (ESR) > 30 mm h<sup>-1</sup>; 3 points for a synovial fluid white blood cell count >3000 cells per  $\mu$ L; 3 points for an increased synovial fluid alpha-defensin (signal-to-cut off ratio >1); 3 points for an elevated synovial fluid leukocyte esterase (++) ; 2 points for polymorphonuclear percentage >80%; and 1 point for synovial CRP >6.9 mg L<sup>-1</sup>.<sup>9</sup> Unfortunately, in infections of synthetic media there are no such rigid and stringent criteria and this makes diagnostics even more difficult. Many orthopaedic surgeons use for the diagnosis of HI the same criteria used in PJIs, however different criteria have been suggested. In 2018, an international consensus established the main criteria for confirming HI which encompasses the presence of a fistula, the presence of pus, two cultural samples suggestive of infection, and the presence of bacteria or fungi in deep sampling, as well. Clinical signs including fever, local inflammation, and local edema as well as radiological signs including osteolysis, seizures, and non-union combined with alteration of inflammatory markers support the diagnosis of HI.<sup>10</sup>

The use of pH as a biomarker for revealing infections is well reported in the literature,<sup>11</sup> indeed Kontinen and co-workers, observed a pH value of 4.38 in the femoral cavity and 5.80 in the femoral stem in the patient with septic loosening.<sup>12</sup> A recent study, reported in 2024 by Judl *et al.* analyzed the pH value of a cohort of 155 patients with the implanted hip (THA;  $n = 85$ ) or knee (TKA;  $n = 70$ ) joint replacements, finding that the group of patients with infection ( $n = 44$ ) had a significantly lower synovial fluid pH (pH =  $6.98 \pm 0.48$ ) than the group of patients with no infection ( $n = 111$ , pH =  $7.82 \pm 0.29$ ,  $p < 0.001$ ). By setting the cut-off level of pH 7.4, the authors found the sensitivity level of infected replacements equal to 88.6% with the specificity level of the measurement equal to 95.5%. The cohort study demonstrated a predictive value of a positive test equal to 88.6% and a predictive value of a negative test equal to 95.5%, confirming the appropriateness of pH measurement in the diagnostic spectrum of hip and knee replacements.<sup>13</sup>

In recent years, there has been a conspicuous surge in the use of wearable and implantable devices for detecting, preventing, and treating different conditions. In the orthopaedic field, Karipott *et al.* reported the important role of implantable wireless sensors in orthopaedic care as valuable analytical tools, for understanding the progression of diseases and injuries.<sup>14</sup>

Furthermore, the advancements in sensors, wireless communication, power management, microelectronics, and other technologies are reducing the technical barrier to constructing reliable implantable wireless sensors.

In the overall scenario of implantable devices for infection monitoring, few examples have been reported in the literature based on electrochemical or optical detection.<sup>15</sup> An interesting example of the first approach has been reported by Tomšik *et al.*, which developed a potentiometric pH sensor based on polyaniline for pH measurement in synovial fluid by depositing chemically the polyaniline on a titanium alloy (Ti-6Al-4V) rod.<sup>16</sup> The second approach is based on the swelling of H<sup>+</sup>-sensitive hydrogels which requires an X-ray source, thus a laboratory set-up instrument.<sup>17</sup> For instance, Arifuzzaman *et al.* evaluated the pH variation through radiography, by measuring the position variation of a radiopaque tungsten rod attached to the disk edges due to the swelling of the hydrogel disk.<sup>17</sup> Only one device has been developed specifically for pH sensing at the orthopaedic hardware level, but unfortunately it is based on the use of X-rays with all the consequences of the case.<sup>18</sup>

Motivated by the need for novel devices for fast and reliable HI management and by our recent article that demonstrated the effectiveness of a point-of-care device to diagnose PJI during surgery in a few minutes,<sup>19</sup> here we investigated the potentiality of the orthopaedic implant to work as sensing tool for fast and in site diagnosis of HI. We selected electrochemically deposited iridium oxide as the sensing element because we previously demonstrated its capability to work in a complex matrix such as whole blood<sup>19</sup> and for its well-known biocompatibility.<sup>20</sup> In this work, a titanium-based orthopaedic implant was directly modified by electrodepositing iridium oxide for pH monitoring (Fig. 1). Thereby, the orthopaedic implant acts both as a fixation of articular fractures, *i.e.* as usually used in the orthopaedic field and as a sensing device for implant-related orthopaedic infection monitoring. To investigate the sensing component of the orthopaedic implant to be used as a pH sensor, iridium oxide was first electrodeposited onto different materials namely titanium, titanium alloy, and stainless steel as well as different components, namely screws and implants. Once selected the functionalized titanium implant as the working electrode, the optimization of the reference electrode was made and the final configuration of the smart sensing orthopaedic implant was tested in standard solutions and bovine serum albumin-containing solution to assess the analytical features of this novel electrochemical device.

## Results and discussion

As a consequence of bacteria colonization onto the implanted device surface, the formation of a biofilm layer happens with the specific role of protecting the colony's survival from the hostile external environment.<sup>21,22</sup> As a result, bacteria grown within the biofilm are highly resistant to the host's immune system and antimicrobial agents, inducing chronic implant-

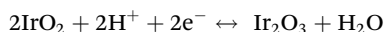


Fig. 1 Orthopaedic titanium-based implant modified with electrodeposited iridium oxide for pH monitoring in HI diagnosis.

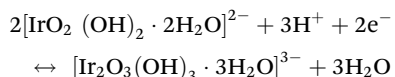
related infections.<sup>23,24</sup> In this newly created environment, the bacteria produce acidic metabolites, such as lactic acid, acetic acid, formic acid, and carbonic acid, with a consequent local pH drop around the implant.<sup>12,24,25</sup> Thus, the detection of pH around the implant is a valuable target analyte for revealing implant-related infections.

With the goal of monitoring pH using miniaturized and user-friendly devices, our research group previously developed potentiometric sensors for (i) pH detection in sweat samples during physical activity<sup>26</sup> and (ii) pH detection in whole blood sampled during orthopaedic surgery.<sup>19</sup> In both cases, the detection is based on the use of screen-printed electrodes modified with iridium oxide as a sensitive layer to H<sup>+</sup> ions.

Indeed, the response of the sensor depends on the H<sup>+</sup> activity and the oxidation state of the deposited iridium, as well. A mixed anhydrous/hydrated iridium oxide film composition is created with the deposition, and the following reactions take place in solution:<sup>27</sup> anhydrous iridium oxide system:



hydrated iridium oxide system:



With the corresponding Nernst equation respectively equal to:

$$E = E^\circ - (2.3RT/2F) \log[\text{Ir}_2\text{O}_3]/[\text{IrO}_2]^2[\text{H}^+]^2$$

$$E = E^\circ - (2.3RT/2F) \log[\text{Ir}_2\text{O}_3]/[\text{IrO}_2]^2[\text{H}^+]^3$$

This means that a variation in the Ir<sup>3+</sup>/Ir<sup>4+</sup> ratio has important consequences on pH sensitivity, producing the observed

super-Nernstian slope, generally known for iridium oxide pH sensors.

Finally, a final potential treatment was performed at +200 mV in pH 7 to ensure a significant amount of both Ir<sup>3+</sup> and Ir<sup>4+</sup> oxidation states.

Furthermore, iridium was selected as an H<sup>+</sup> sensing material due to its biocompatibility, which has been demonstrated in various studies,<sup>28–31</sup> making it suitable for functionalizing implanted orthopaedic devices. In detail, cytotoxicity assessments conducted on the specific material demonstrate that iridium oxide exhibits minimal cytotoxicity, with cell viability higher than 70%,<sup>28,29</sup> a threshold set by the ISO standard 10993-5:2009.

Following this approach, in the present work, a titanium-based orthopaedic implant was directly modified by electrodepositing iridium oxide for pH monitoring, with the aim to be used as a smart tool for HI diagnosis in the orthopaedic field.

#### Investigation of material type for the working electrode

Different commercially available orthopaedic tools were investigated as working electrodes to be used as implantable pH sensors. For this purpose, medical screws and orthopaedic implants fabricated with different materials were evaluated in this study. Indeed, plates and screws are used to reduce the fracture, then stabilize it through different biomechanical concepts depending on the case.

Furthermore, the materials of the orthopaedic tools, *i.e.* titanium, cobalt–chromium–molybdenum alloy, and stainless steel, are commonly used for the fabrication of these types of equipment, as they are characterized by high mechanical resistance and biocompatibility.<sup>32,33</sup>

To make the orthopaedic devices sensitive to pH, both screws and implants were modified with iridium oxide following the protocol previously optimized.<sup>19,26</sup> Iridium electrodeposition was carried out onto the orthopaedic tool surface, and potentiometric measurements were performed in the range of pH 4–8, using a screen-printed Ag/AgCl as pseudo-reference electrode.

In the initial study, screws fabricated with stainless steel, titanium alloy, and titanium were first tested (Fig. 2a). In detail, using the stainless-steel screw a sensitivity equal to  $-(0.092 \pm 0.004)$  V pH<sup>-1</sup> unit, with  $R^2 = 0.975$  was obtained, while using the titanium-based screw a sensitivity equal to  $-(0.061 \pm 0.002)$  V pH<sup>-1</sup> unit, and  $R^2 = 0.992$  were obtained. Finally, using the titanium alloy screw, a sensitivity equal to  $-(0.058 \pm 0.004)$  V pH<sup>-1</sup> unit, with  $R^2 = 0.957$ , was recorded. The recorded variations can be ascribed to the different behaviour of the used materials in terms of adhesion of the electrodeposited iridium oxide.<sup>34,35</sup> To this regard, Marzouk<sup>35</sup> investigated a variety of pure metals, such as Au, Ag, Ti, Cu, Ni, W, Zr, Co, and alloys, such as stainless steel, nickel–chrome, and Hastelloy to understand how the different materials can affect iridium oxide electrodeposition. In detail, the authors considered the appropriate extent of iridium oxide adhesion, the resistance to wiping with tissue paper, the stability of the cyclic voltammograms known for iridium oxide during several potential cycles, and the visual examination of blue iridium oxide deposits, obtaining that titanium and stainless steel are the most suitable materials for iridium oxide electrodeposition.

Additionally, the use of a screw as a sensing device has limitations concerning (i) its limited sensing area compared to the implantable device and (ii) the possibility of damaging the modified surface of the screw during the insertion into the implant.

For these reasons, the implant of titanium material was then investigated to deliver an implantable device to sense the decrease of pH in the whole implantable device area.

Considering the correlation coefficient and the literature,<sup>34,35</sup> titanium was selected as the material for further studies.

As previously performed for the screw, the iridium oxide was electrodeposited directly onto the implant surface, and measurements were carried out in standard solutions using a screen-printed Ag/AgCl pseudo-reference electrode.

A linear correlation between pH and potential was obtained in the pH range 4–8, with a calibration curve equation equal to  $y = (0.72 \pm 0.01) - (0.076 \pm 0.002)x$ ,  $R^2 = 0.998$  (Fig. 2b).

Considering the obtained results, the orthopaedic implant was further investigated to be used as a working electrode for the pH measurements in the rest of the work.

### Study of the reference electrode

Concerning the final goal of the implant to perform the potentiometric pH measurement directly implanted into the body, we investigated the use of the proper reference electrode. Indeed, the choice of the reference electrode is highly relevant to obtaining an implantable sensing device characterized by

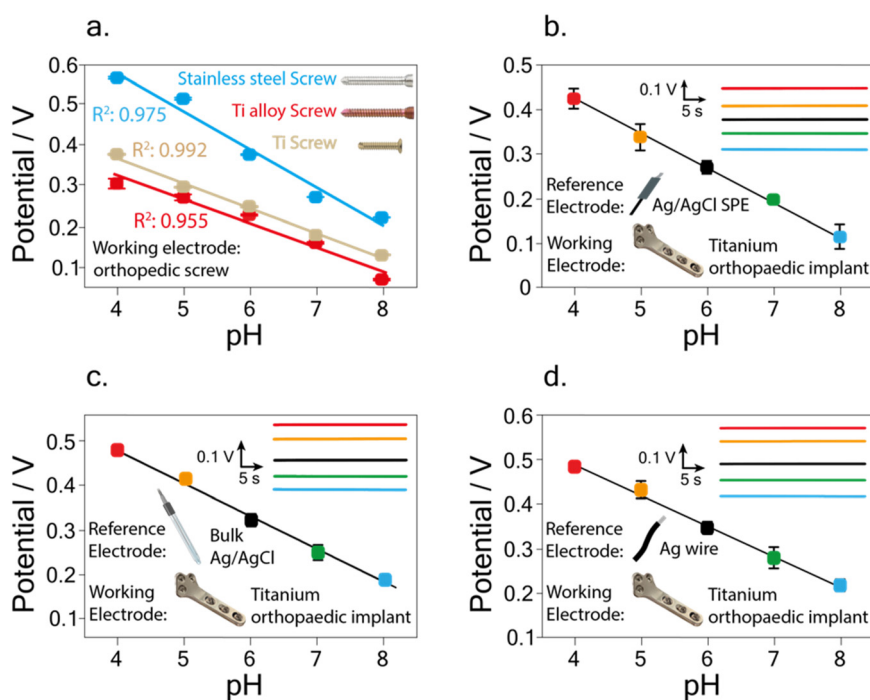


**Fig. 2** Calibration curves performed using as working electrode the stainless-steel screw (blue), the titanium alloy screw (red), and the titanium screw (brown), using as reference electrode the screen-printed Ag/AgCl pseudo reference electrode (a). Calibration curve and relative potentiograms (insets) carried out using as a working electrode the titanium orthopaedic implant and as reference electrodes the screen-printed Ag/AgCl pseudo reference electrode (b), the bulk Ag/AgCl reference electrode (c), and the wire Ag wire electrode (d).

small dimensions, easiness of introduction in the fractured bone area, and biocompatibility. Additionally, long-term analysis requires stable signal acquisition, typically given by bulky and rigid electrodes.<sup>36</sup> Nevertheless, the dimensions and fragilities of these electrodes are not suitable for the development of implantable sensor devices. For these reasons, we investigate the use of three different reference electrodes, by comparing the screen-printed Ag/AgCl pseudo-reference electrode (used for the previous analyses) with bulk Ag/AgCl reference electrode as a reference measurement, and with a wire Ag reference electrode. The use of the wire Ag reference electrode is mainly due to the final goal to deliver a sensor placed directly in the infection zone characterized by easy implantability, long-term stability, and easy connectivity.

Calibration curves were performed in standard solution using the modified titanium implant as the working electrode and each of the aforementioned electrodes as reference electrodes.

In detail, as previously reported (Fig. 2b) the use of the screen-printed Ag/AgCl pseudo-reference electrode gave a linear correlation between pH and potential in the pH range 4–8, with a calibration curve equation equal to  $y = (0.72 \pm 0.01) - (0.076 \pm 0.002) x$ ,  $R^2 = 0.998$ . Reproducibility was evaluated by carrying out measurements of pH 7 using three different implants, obtaining a relative standard deviation (RSD %) equal to 9.0%. Using the bulk Ag/AgCl reference electrode a linear correlation between pH and potential was obtained in the pH range 4–8, with a calibration curve equation equal to  $y = (0.78 \pm 0.02) - (0.073 \pm 0.003) x$ ,  $R^2 = 0.995$  (Fig. 2c). The RSD % was performed by carrying out measurements of pH 7 using three different implants, resulting equal to 10.7%.

Finally, carrying out the measurements with the wire Ag reference electrode a linear correlation between pH and potential was obtained in the pH range 4–8, with a calibration curve equation equal to  $y = (0.76 \pm 0.02) - (0.068 \pm 0.002) x$ ,  $R^2 = 0.996$  (Fig. 2d). The RSD % calculated by measuring pH 7 using three different implants was equal to 8.6%, corresponding to a standard deviation of 0.024 V.

Noteworthy, compared to the calibration curve obtained using the bulk Ag/AgCl reference electrode, the use of the wire Ag reference electrode showed no significant variation in the recorded slope within the experimental error.

The recorded super-Nernstian slope (*i.e.*,  $-(0.068 \pm 0.002) \text{ V pH}^{-1}$  unit) is commonly obtained when using an electrodeposited iridium oxide film as a sensitive pH layer and is a direct effect of the oxide layer composition system.<sup>37,38</sup> In detail, the recorded slope with the developed iridium oxide-modified implant results in agreement with the one obtained for pH detection using titanium-based electrodes modified with iridium oxide, namely  $-(0.074 \pm 0.001) \text{ V pH}^{-1}$  unit.<sup>35</sup> A similar finding was also observed by comparison with different working electrode materials, namely platinum micro-electrodes,<sup>39</sup> graphite-based SPE,<sup>40</sup> and ink-jet printed platinum nanoparticles,<sup>41</sup> with a slope equal to  $-(0.0729 \pm 0.0009) \text{ V pH}^{-1}$  unit,  $-(0.0744 \pm 0.0008) \text{ V pH}^{-1}$  unit, and  $-(0.0713 \pm 0.0003) \text{ V pH}^{-1}$  unit, respectively. This observation demon-

strates the reliability of the implant modification procedure applied in this study.

A deep analysis was finally carried out to investigate the stability of the measurements by assessing the pH 7 in continuous analysis for 120 min. Indeed, long-term stability is a crucial parameter for real-time analyses performed by an implanted sensor.

As depicted in Fig. S1a† a slight decrease in the signal equal to 0.0163 V after 120 min was recorded using the modified orthopaedic implant as the working electrode and the screen-printed Ag/AgCl as the reference electrode. An even lower decrease was recorded using the bulk Ag/AgCl reference electrode, with a potential drift equal to 0.0056 V after 120 min (Fig. S1b†). Finally, the measurement performed with the wire Ag reference electrode gave the lowest drift equal to +0.0026 V (Fig. S1c†).

Nevertheless, considering the time range from 30 minutes up to 2 h, a negligible potential drift equal to 0.00017 V is obtained, thus after 30 minutes this configuration allows for the lowest drift, highlighting the superior performances of the sensing device based on the use of the wire Ag reference electrode in terms of potential drift.

The use of wire Ag is in agreement with the literature related to different electrochemical implantable devices, as reported for instance by Idili *et al.*,<sup>42</sup> Li *et al.*,<sup>43</sup> and Gil *et al.*<sup>44</sup>

In summary, comparing the results, similar performances among the three different reference electrodes in terms of sensitivity, reproducibility, and correlation coefficients of the calibration curves were obtained. Additionally, as the final goal is to deliver an implantable sensor, considering physical parameters such as size and flexibility, the wire Ag electrode was selected as the reference electrode for further analyses.

### Morphological characterization

To get inside the morphology of the titanium implant surface, a deep investigation through FE-SEM analysis was carried out on the bare and the modified sample surfaces. EDX analysis was also employed to assess the presence and distribution of iridium oxide on the surface of the modified sample.

Fig. 3a and b depict the bare titanium sample at different magnitudes: a smooth surface can be observed. The EDX spectrum is reported in Fig. 3c and two strong peaks around 5 keV are ascribable to Ti.

A similar smooth surface is also observed in the presence of the iridium oxide-modified surface. No cracks or signs of delamination can be observed after the modification (Fig. 3d), indicating the growth of an even, well-adhered iridium oxide layer. Furthermore, the presence of micro-sized agglomerates, observed as light grey spots at higher magnitudes on the sample surface (Fig. 3e), is probably due to residues of electrolytes present in the solution used for iridium electrodeposition. EDX spectrum in Fig. 3f shows a low intense peak at 9 keV, highlighting the presence of iridium on the modified titanium sample surface.

An EDX mapping analysis was performed at a lower magnitude, on the modified implant zone shown in Fig. 3g, showing

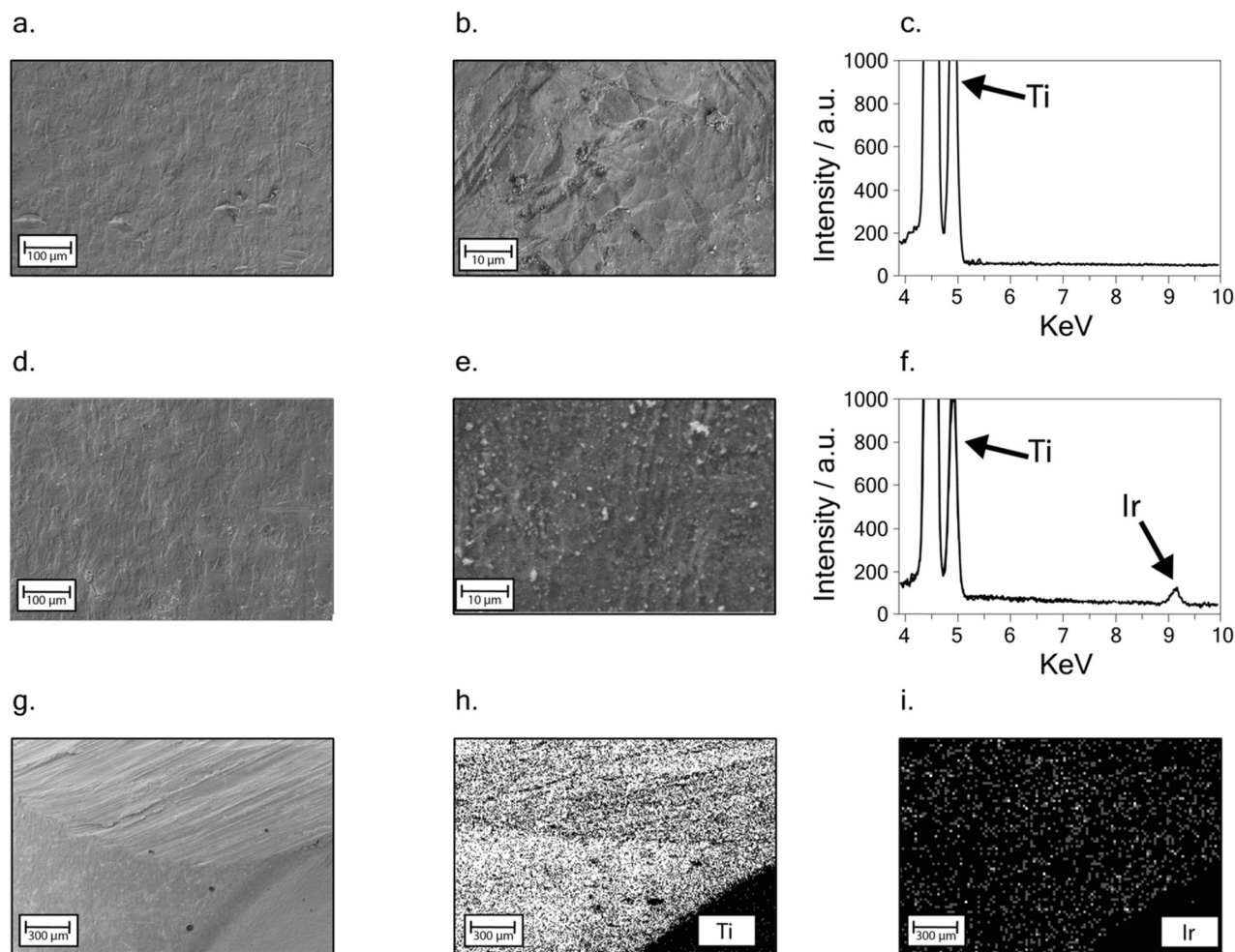


**Fig. 3** FE-SEM micrographs at different magnitudes of the bare titanium implant surface (a and b); EDX spectrum between 4 and 10 keV recorded on the bare titanium implant surface (c). FE-SEM micrographs at different magnitudes of the titanium implant surface after electrodeposition (d and e). EDX spectrum between 4 and 10 keV recorded on the titanium implant surface after electrodeposition (f). FE-SEM micrograph showing a detail of the electrodeposited titanium implant sample used for EDX mapping analysis (g). EDX mapping results showing the distribution of Ti signal (h). EDX mapping results showing the distribution of Ir signal (i). (No EDX signal was collected from the lower right corner of the picture, as that part of the sample was not oriented toward the detector).

an edge of the sample. Ti and Ir distributions (Fig. 3h–i) confirmed the iridium oxide uniform distribution, even when compared with chlorine and potassium signal, resulting from salt residues, as highlighted in Fig. S2.†

### Analytical performances

A crucial element in developing the new implanted sensors is to deliver a high-performance device in terms of reproducibility of measurements, as the orthopaedic implant is a not-commonly employed material for working electrode fabrication. Reproducibility was evaluated by carrying out measurements of pH 7 using the same orthopaedic implant (intra-electrode analyses) and using three different implants (inter-electrode analyses). A relative standard deviation equal to 1.7% ( $n = 3$ ) and 8.6% ( $n = 3$ ) was obtained for intra and inter-electrode assessment, respectively, highlighting the good reproducibility of the obtained measurements.

To deliver a sensor ready to use, the storage stability of the iridium oxide-modified implant was evaluated by conducting measurements in a buffer solution at pH 7. In detail, pH detection was carried out on the same day as the iridium oxide electrodeposition, and after 1, 2, 3, and 4 weeks, the implant was stored under vacuum at  $-27\text{ }^{\circ}\text{C}$ .<sup>26</sup> Fig. S1d† shows a slight decrease in the potential after four weeks, with a difference of 0.018 V compared to the potential recorded the same day of the iridium oxide electrodeposition.

Nonetheless, considering the time range starting from the first week and up to the last investigated week (*i.e.*, after four weeks from the electrodeposition) a minimal signal decrease was recorded equal to 0.007 V, which corresponds to a potential change from 0.268 V (week 1) to 0.261 V (week 4), and to a pH change from 7.23 to 7.34. Based on the research activity in the industrial field for the development of (bio)sensors, a specific time after the fabrication is needed for their stabiliz-

ation. Afterwards, the devices can be commercialized. Following these findings, the herein-developed sensor can be implanted after a “stabilization time” of one week.

To assess the reliability of the Ag wire electrode and to understand the effect of the presence of chloride ions on the Ag reference electrode, we carried out measurements by testing the developed pH sensor at chloride concentrations equal to 50 mM, 100 mM, and 150 mM, taking into account the blood physiological value of 98–107 mM.<sup>45</sup> As depicted in Fig. S1e,† the measurements carried out in the absence and the presence of different concentrations of chloride ion did not show any significant variation within the experimental error, demonstrating the robustness of the sensor.

Additionally, to assess the reliability of the developed sensor, measurements were carried out (i) by using the implant completely immersed in Britton Robinson buffer solution at pH 7 and 5 (*i.e.* both the 5 cm modified surface of the implant and the 5 cm unmodified surface of the implant) and (ii) using the implant immersed only by the iridium modified surface (as performed for the measurements throughout the whole manuscript).

As depicted in Fig. S1f† any potential difference was recorded using the investigated set-up, highlighting the negligible effect of the presence of unmodified surfaces.

Furthermore, to evaluate the sensor's reliability for analysis in the real matrix, the interference study was conducted to evaluate the selectivity of the developed sensor in the presence of different contents of chloride ions as well as interfering compounds usually found in blood samples. For this investigation, potentiometric measurements were carried out by

testing Britton–Robinson buffer at pH 7.4, in the presence of 334 mg dL<sup>-1</sup> Na<sup>+</sup>,<sup>45</sup> 2.5 mg dL<sup>-1</sup> Mg<sup>2+</sup>,<sup>45</sup> 5.5 mg dL<sup>-1</sup> Ca<sup>2+</sup>,<sup>45</sup> 5 mg dL<sup>-1</sup> bovine serum albumin (BSA),<sup>45</sup> 100 mg dL<sup>-1</sup> glucose,<sup>45</sup> and 43 mg dL<sup>-1</sup> urea,<sup>45</sup> As depicted in Fig. 4b no significant variations were recorded in the presence of these interferent ions and molecules, highlighting the selectivity of the developed sensor.

Finally, to investigate the possible memory effect during real measurements, hysteresis studies were carried out. Measurements were conducted in buffer solutions at different pH, namely pH 8, pH 7, pH 6, pH 5, and 4, and *vice versa*. Fig. 4c depicts the potentiograms obtained for this study, showing the absence of hysteresis effects, allowing accurate pH measurements without any memory effect.

#### Analyses in BSA solution

Taking into account the final purpose of the sensor to be applied for real-time analysis and implanted into the patient's body, a preliminary study was performed. In detail, following the study conducted on the possible interference of compounds on pH detection, a deeper analysis was focused on testing the developed sensor in buffer solutions containing 5 mg dL<sup>-1</sup> of BSA.<sup>45</sup> Indeed, BSA is commonly used as a biological fouling standard to test the possible interference deriving from fouling.<sup>46–48</sup>

A linear relation between pH and potential was obtained in the pH range of 4–8, using buffer solutions with a BSA concentration of 5 mg dL<sup>-1</sup>. The calibration curve was equal to  $y = (0.75 \pm 0.008) - (0.070 \pm 0.001) x$ ,  $R^2 = 0.999$  (Fig. 5a). The RSD % was performed by carrying out measurements of pH 7 using

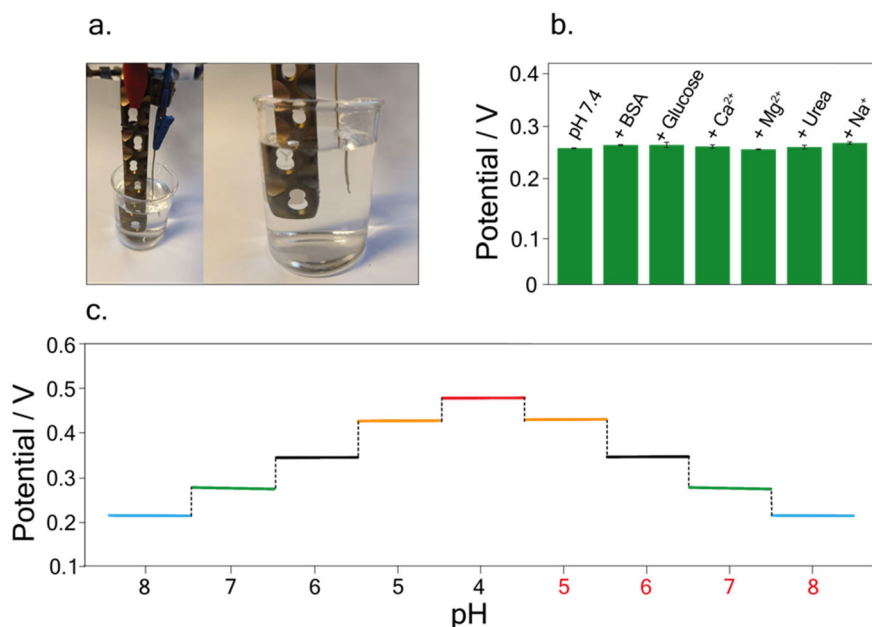


**Fig. 4** Picture of the developed tool for pH detection, comprising the iridium-modified titanium-based implant, and the wire reference electrode (a). Histogram bars obtained for the potentiometric measurements of Britton–Robinson buffer at pH 7.4, in the presence of 334 mg dL<sup>-1</sup> Na<sup>+</sup>, 2.5 mg dL<sup>-1</sup> Mg<sup>2+</sup>, 5.5 mg dL<sup>-1</sup> Ca<sup>2+</sup>, 5 mg dL<sup>-1</sup> BSA, 100 mg dL<sup>-1</sup> glucose, and 43 mg dL<sup>-1</sup> urea (b). Hysteresis study testing different pH values from 8 to 4 and *vice versa* in the selected working conditions (c).



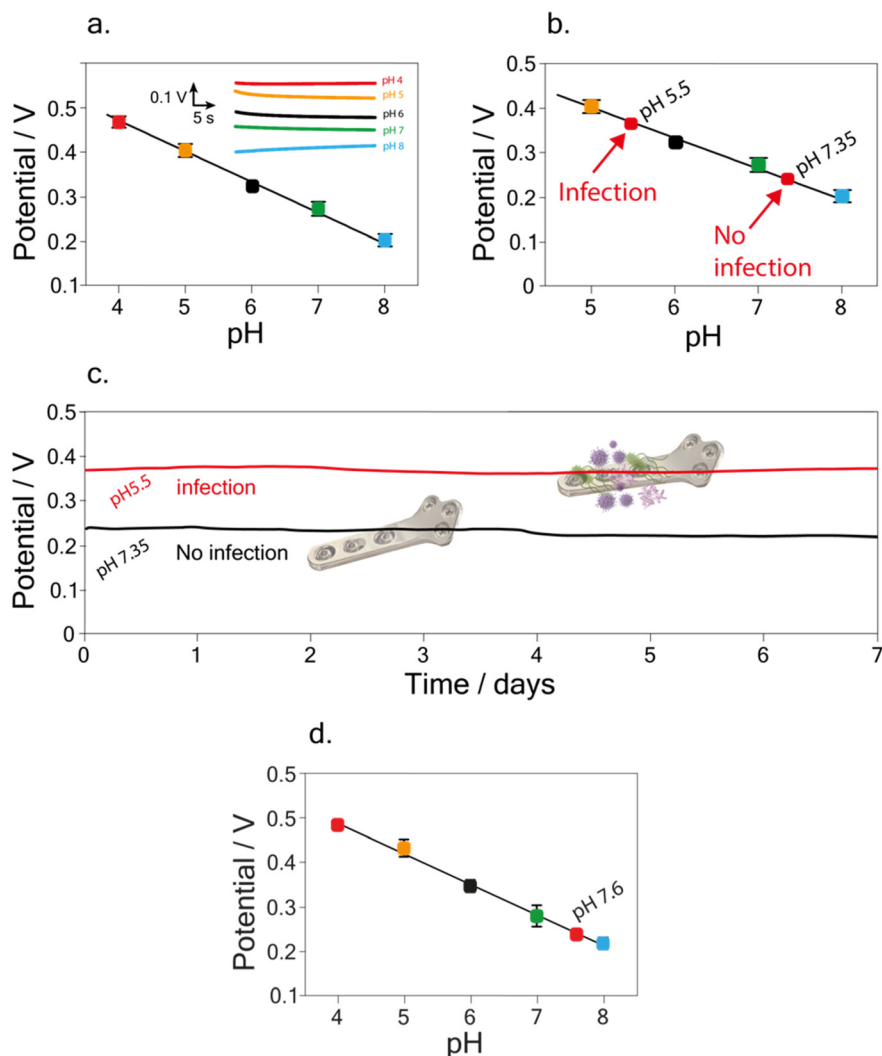


**Fig. 5** Calibration curve performed in Britton–Robinson buffer solutions containing BSA 5 mg dL<sup>-1</sup>, in the pH range from 4 to 8 (a), and relative potentiograms (inset). Recovery studies carried out in buffer solutions containing BSA 5 mg dL<sup>-1</sup>, for the assessment of the selected pH values, namely pH equal to 5.5 (infection) and pH equal to 7.35 (no infection) (b). Continuous potentiometric measurement for pH detection carried out by immersing the iridium-modified implant sensor for one week in not infected samples (Britton–Robinson buffer solution at pH 7.35 + BSA 5 mg dL<sup>-1</sup>) and infected samples (buffer solution at pH 5.5 + BSA 5 mg dL<sup>-1</sup>) (c). Calibration curve performed in Britton–Robinson for the detection of pH in synovial fluid extracted from healthy patients (d).

the same implant, resulting equal to 0.5%. Noteworthy the obtained slope in the BSA solution is comparable with the one obtained in the standard solution, namely,  $(0.068 \pm 0.002)$  V pH<sup>-1</sup> unit, highlighting the reliability of the developed sensor.

To further assess the accuracy of the developed sensor, recovery studies were performed in the BSA solution. A recovery percentage equal to  $(99 \pm 2)$  % and  $(99.2 \pm 0.3)$  % was calculated for pH 7.35 and pH 5.5 (Fig. 5b), namely the value of pH in physiological<sup>45</sup> and during infection<sup>12,16</sup> conditions, respectively.

A final study was carried out in order to evaluate the matrix effect of the developed sensor, due to the potential absorption of the proteins causing fouling problem. In detail, pH detection was performed in Britton–Robinson buffer solution + KCl 0.145 M + 5 mg dL<sup>-1</sup> of BSA at pH 7.35 and pH 5.5. As shown

in Fig. 5c, conducting the measurements continuously for one week, the sensor exhibits negligible drift effect in the BSA solution, in agreement with the previous data obtained for drift evaluation in the Britton–Robinson buffer solution, pH 7. In detail, a potential drift equal to 0.013 V and 0.014 V was calculated after one week of measurements, for pH 5.5 and 7.35 respectively.

Finally, the potential applicability of the developed implant device in a different matrix was assessed by measuring pH in synovial fluid *i.e.* a biofluid usually analyzed in the case of the periprosthetic joint infection. We tested a synovial fluid extracted from healthy patients, finding a pH equal to  $7.7 \pm 0.1$  using the developed implant device, which agrees with the value *i.e.*  $7.9 \pm 0.1$  obtained using pH-meter. This demonstrates the potential of the application as an implantable

**Table 1** Implantable devices reported in the literature for HI and PJI monitoring

Analytical technique	Sensing element	Working electrode	Sensor configuration	Instrumentation	pH Linear range	Matrix	Ref.
Potentiometry	Electrodeposited polyaniline film	Titanium alloy (Ti-6Al-4V) rod	Rod to be probably embedded with orthopaedic implant	6-Channel high input impedance voltmeter	pH 5–8	Standard solution with BSA	16
Radiographic measurements	Polyacrylic (AAc-co-n-OA) hydrogel film	Orthopaedic implant	As support to embed hydrogel swelling, sensor attached to an orthopaedic implant fixed to a cadaveric tibia	X-ray imaging instrument	pH 4–8	Buffer solution	17
Radiographic measurements	Polyethylene glycol and bromocresol green dye hydrogel film	Orthopaedic implant	Sensor based on bottom layer of scintillator particles and top layer with bromocresol green dye. The 3D printed holder was attached on a tibial orthopaedic plate	X-ray imaging instrument	pH 3–8	Buffer solution	18
Radiographic measurements	Polyacrylic (AAc-co-n-OA) hydrogel film	Orthopaedic implant	As support to embed hydrogel swelling, sensor attached to prosthetic implant	X-ray imaging instrument	pH 4–8	Bovine synovial fluid	49
Potentiometry	Electrodeposited iridium oxide	Orthopaedic implant	No additional embedding part, because the orthopaedic implant works itself as the sensing tool	Portable potentiostat	pH 4–8	Standard solution with BSA	This work

device even when compared with the few examples reported in the literature related to both electrochemical and optical implantable devices for PJI and HI monitoring. Indeed, as highlighted in Table 1, the here-developed device is able to render the whole implant potentially sensitive to HI monitoring when compared with the one developed by Tomšik *et al.*,<sup>16</sup> and does not require a laboratory-set up for analyses as reported by Arifuzzaman *et al.*, Uzair *et al.*, and Wijayaratna *et al.*<sup>17,18,49</sup>

## Experimental

### Reagents and materials

Iridium(IV) chloride, hydrogen peroxide, oxalic acid, sodium carbonate, anhydrous potassium carbonate potassium dihydrogen phosphate, dipotassium hydrogen phosphate, sodium hydroxide, acetic acid, boric acid, potassium chloride, magnesium chloride, sodium chloride, calcium chloride, bovine serum albumin were purchased from Sigma Aldrich. Stainless steel screw (ref. 204.820, length 20 mm), Commercially Pure (CP) titanium screw (ref. 404.810, length 20 mm), titanium alloy screw (TiAl<sub>6</sub>Nb ref. 04.211.020, length 20 mm), and orthopaedic implants (CP titanium, length 10 cm) were provided by Gemelli Hospital and purchased from Johnson and Johnson, DePuy Synthes. Silver Wire 99.99% 0.1 mm diameter (AG00-WR-000116) was purchased by Goodfellow. The wire (total length 5 cm) was covered with a shrink tube, while the two ends (5 mm) of the wire were not covered with the tube, to allow the connection with the potentiostat and the immersion in solution for the electrochemical measurements, respectively.

### Electrochemical sensor assembly and modification

The three-electrode systems used for electrochemical pH detection consist of different combinations of working electrodes and reference electrodes to optimize the analytical performances and cost-effectiveness. Working electrodes such as screws and implants are paired with various reference electrodes, including Ag/AgCl-screen printed electrode, Ag-wire, and Ag/AgCl-bulk reference electrode. These combinations are chosen to establish the best experimental setup for pH detection.

### Orthopaedic-based sensor modification

The iridium oxide film, which is sensitive to pH variations, was electrochemically deposited onto orthopaedic-based implants or screws using the cyclic voltammetry technique. In detail, the iridium-containing solution was prepared in agreement with Ges *et al.*<sup>50</sup> Briefly, 75 mg of iridium(IV) chloride were dissolved in 50 mL of distilled water and stirred for 15 minutes. Then 0.5 mL of 30 w/w H<sub>2</sub>O<sub>2</sub> was added and stirred for 10 minutes, followed by the addition of 250 mg oxalic acid, with a further 10 minutes of stirring. The resulting solution was adjusted to pH 10.5 with anhydrous potassium carbonate and allowed to stabilize at room temperature for 2 days.

Electrodeposition was carried out by partially immersing the working electrodes (namely screws 0.5 cm or implant 5 cm), and a combined electrode (platinum tip counter, Ag/AgCl reference electrode) (Amel electrochemistry, 805/CPG/6) in the iridium-containing solution. Subsequently, 60 cycles of cyclic voltammetry between 0 and 0.8 V, with a step potential of 0.05 V and a scan rate of 0.05 V s<sup>-1</sup> were carried out for the

electrodeposition of the iridium oxide onto the working electrode.

The cathodic charge storage capacity (CSC), which is equivalent to all the available  $\text{Ir}^{4+}$  on the substrate, was calculated according to Meyer *et al.*,<sup>34</sup> and was found equal to  $0.6 \text{ mC cm}^{-2}$ . This value is in the range reported in the literature using different materials including stainless steel, Au, and Pt.<sup>34,51</sup>

Before conducting potentiometric measurements, the orthopaedic-based sensor underwent treatment involving the application of a constant potential of 200 mV for 5 minutes. This treatment is needed to stabilize the composition of  $\text{Ir}^{3+}/\text{Ir}^{4+}$  on the electrode surface, thereby enhancing the analytical performances in terms of reproducibility and long-term stability.

### Electrochemical measurements in standard solution

pH measurements were performed by using the proposed orthopaedic-based sensor, which includes an orthopaedic implant or screws as a working electrode, and each of the aforementioned electrodes as reference electrodes, connecting them to a portable PalmSens4 potentiostat. In detail, potentiometric measurement of pH was carried out by immersing the two-electrode system in a beaker containing 50 mL of standard solution at a known pH, obtaining the signal in less than 10 s.

To measure possible current leakages in the circuit, the current was measured by connecting a Fluka 289 multimeter to the working electrode, *i.e.* modified orthopaedic implant, and reference electrode, *i.e.* Ag wire, immersed in the Britton Robinson buffer solution at pH 7, observing no flowing current in the equivalent circuit higher than 20 nA (the minimum current readable by the instrumentation).

### Electrochemical measurements in standard solutions containing BSA

pH measurements were performed by using the iridium-modified titanium implant as the working electrode, and the Ag wire as the reference electrode, connecting them to a portable PalmSens4 potentiostat. The potentiometric detection of pH was carried out by immersing the two-electrode system in a beaker containing 50 mL of Britton–Robinson buffer solutions at a known pH, containing  $5 \text{ mg dl}^{-1}$  of BSA.

### Morphological analyses

Micrographs of the not-modified and the iridium-modified titanium implant were acquired using a field emission scanning electron microscope (FE-SEM) Leo SUPRA™ 35 (Carl Zeiss SMT, Oberkochen, Germany). Energy-dispersive X-ray spectroscopy (EDX) was performed by means of an INCASight, 7426 apparatus by Oxford Instruments.

## Conclusions

Reduction of readmissions, revision procedures, and recovery time can all be achieved with early detection of any decrease

in implant function and subsequent appropriate intervention. However, before they are incorporated into clinical practice, there are a number of important obstacles to be addressed, including those pertaining to biocompatibility, customization, and implant dependability in conjunction with sensors. In 2022 in a review published in Chemical Review Journal, the authors highlighted the absence of a sensor-integrating orthopaedic implant device that was used in clinical practice up to 2022,<sup>52</sup> in 2024 a physical sensor-integrating orthopaedic implant has been recently reported in the market of orthopaedic implant,<sup>53</sup> demonstrating the reliability of the sensorized orthopaedic implant. If the ongoing market example relies on the monitoring of the physical integrity of the orthopaedic implant, a smart sensorized orthopaedic implant to promptly reveal the infection could have a huge impact in the orthopaedic field, considering the important issue of HI, as reported in the introduction, as well as the necessity to reduce the overuse of antibiotics. We demonstrated, for the first time to our knowledge, that the actually used orthopaedic implant can be easily functionalized with iridium oxide film to work as a sensing implant, thus with a simple addition process of electrodeposition, the ongoing orthopaedic implant could work as a working electrode. The further step requires the assembling of a battery-free RFID device<sup>26,54</sup> for data acquisition and management to deliver a reliable and effective implantable diagnostic tool for fast identification of HI with the overriding goal to take the correct countermeasure in a timely fashion.

## Author contributions

The manuscript was written with contributions from all authors. L. F.: investigation, methodology, data curation, writing, review, and editing; V. M.: writing original draft, data curation, methodology, writing, review, and editing; C. G.: investigation, formal analysis; L. D.: SEM investigation, writing, review, and editing; R. V.: writing, review and editing; G. M.: funding acquisition; F. A.: conceptualization, writing original draft, review and editing, funding acquisition. All authors have read and agreed to the published version of the manuscript.

## Conflicts of interest

Authors declare no conflicts of interest.

## Acknowledgements

This work was supported by JPIAMR Joint Programming Initiative on Antimicrobial Resistance, project “Innovative multiplex paper-based electrochemical biosensor and artificial intelligence for smart periprosthetic joint infection and AMR diagnostic” (SENSIF) project.

## References

- 1 [https://health.ec.europa.eu/antimicrobial-resistance/eu-action-antimicrobial-resistance\\_en](https://health.ec.europa.eu/antimicrobial-resistance/eu-action-antimicrobial-resistance_en) (accessed February 12, 2024).
- 2 T. F. Moriarty, L. G. Harris, R. A. Mooney, J. C. Wenke, M. Riool, S. A. J. Zaat, A. Moter, T. P. Schaer, N. Khanna, R. Kuehl, V. Alt, A. Montali, J. Liu, S. Zeiter, H. J. Busscher, D. W. Grainger and R. G. Richards, *J. Orthop. Res.*, 2019, **37**, 271–287.
- 3 E. Clayman, Z. Beauchamp and J. Troy, *ePlasty*, 2023, **23**, e1.
- 4 R. V. Thakore, S. E. Greenberg, H. Shi, A. M. Foxx, E. L. Francois, M. A. Prablek, S. K. Nwosu, K. R. Archer, J. M. Ehrenfeld, W. T. Obremsky and M. K. Sethi, *J. Clin. Orthop. Trauma*, 2015, **6**, 220–226.
- 5 H. Serrier, C. Julien, C. Batailler, E. Mabrut, C. Brochier, S. Thevenon, M. Maynard-Muet, A. Henry, S. Lustig, L. Huot, T. Ferry and The Lyon Bji Study group, *Front. Med.*, 2021, **8**, 552669.
- 6 E. M. Zardi and F. Franceschi, *J. Infect. Public Health*, 2020, **13**, 1888–1891.
- 7 N. Walter, B. Wimalan, S. Baertl, S. Lang, T. Hinterberger, V. Alt and M. Rupp, *BMC Nurs.*, 2022, **21**, 190.
- 8 T. F. Moriarty, R. Kuehl, T. Coenye, W.-J. Metsemakers, M. Morgenstern, E. M. Schwarz, M. Riool, S. A. J. Zaat, N. Khana, S. L. Kates and R. G. Richards, *EFORT Open Rev.*, 2016, **1**, 89–99.
- 9 J. Parvizi, T. L. Tan, K. Goswami, C. Higuera, C. Della Valle, A. F. Chen and N. Shohat, *Arthroplasty*, 2018, **33**, 1309–1314.e2.
- 10 W. Metsemakers, M. Morgenstern, M. A. McNally, T. F. Moriarty, I. McFadyen, M. Scarborough, N. A. Athanasou, P. E. Ochsner, R. Kuehl, M. Raschke, O. Borens, Z. Xie, S. Velkes, S. Hungerer, S. L. Kates, C. Zalavras, P. V. Giannoudis, R. G. Richards and M. H. J. Verhofstad, *Injury*, 2018, **49**, 505–510.
- 11 T. J. Kinnari, J. Esteban, N. Z. Martin-de-Hijas, O. Sánchez-Muñoz, S. Sánchez-Salcedo, M. Colilla, M. Vallet-Regí and E. Gomez-Barrena, *J. Med. Microbiol.*, 2009, **58**, 132–137.
- 12 Y. T. Konttinen, M. Takagi, J. Mandelin, J. Lassus, J. Salo, M. Ainola, T.-F. Li, I. Virtanen, M. Liljeström, H. Sakai, Y. Kobayashi, T. Sorsa, R. Lappalainen, A. Demulder and S. Santavirta, *J. Bone Miner. Res.*, 2001, **16**, 1780–1786.
- 13 T. Judl, S. Popelka, E. Tomšík, M. Hrubý, M. Daniel, J. Fojt, P. Melicherčík, I. Landor and D. Jahoda, *J. Clin. Med.*, 2024, **13**, 688.
- 14 S. S. Karipott, B. D. Nelson, R. E. Guldborg and K. G. Ong, *Expert Rev. Med. Devices*, 2018, **15**, 255–264.
- 15 V. Mazzaracchio, R. Vitiello, G. Maccauro and F. Arduini, *TrAC, Trends Anal. Chem.*, 2024, **172**, 117544.
- 16 E. Tomšík, K. Gunár, T. Krunclová, I. Ivanko, J. Troustil, J. Fojt, V. Hybášek, M. Daniel, J. Sepitka, T. Judl, D. Jahoda and M. Hrubý, *Adv. Mater. Interfaces*, 2023, **10**, 2201878.
- 17 Md. Arifuzzaman, P. W. Millhouse, Y. Raval, T. B. Pace, C. J. Behrend, S. Beladi Behbahani, J. D. DesJardins, T.-R. J. Tzeng and J. N. Anker, *Analyst*, 2019, **144**, 2984–2993.
- 18 U. Uzair, D. Benza, C. J. Behrend and J. N. Anker, *ACS Sens.*, 2019, **4**, 2367–2374.
- 19 L. Fiore, R. Vitiello, A. Perna, G. Maccauro and F. Arduini, *Microchem. J.*, 2022, **183**, 108061.
- 20 S. C. Mailley, M. Hyland, P. Mailley, J. M. McLaughlin and E. T. McAdams, *Mater. Sci. Eng., C*, 2002, **21**, 167–175.
- 21 A. B. Estrela and W.-R. Abraham, *Pharmaceuticals*, 2010, **3**, 1374–1393.
- 22 E. Seebach and K. F. Kubatzky, *Front. Immunol.*, 2019, **10**, 1724.
- 23 J. M. Schierholz and J. Beuth, *J. Hosp. Infect.*, 2001, **49**, 87–93.
- 24 S. B. Behbahani, S. D. Kiridena, U. N. Wijayaratna, C. Taylor, J. N. Anker and T.-R. J. Tzeng, *Front. Microbiol.*, 2022, **13**, 1028560.
- 25 A. Ghimire and J. Song, *ACS Appl. Mater. Interfaces*, 2021, **13**, 20921–20937.
- 26 V. Mazzaracchio, L. Fiore, S. Nappi, G. Marrocco and F. Arduini, *Talanta*, 2021, **222**, 121502.
- 27 S. Carroll and R. P. Baldwin, Self-calibrating microfabricated iridium oxide pH electrode array for remote monitoring, *Anal. Chem.*, 2010, **82**, 878–885.
- 28 J. Selvakumaran, M. P. Hughes, J. L. Keddie and D. J. Ewins, in 2nd Annual International IEEE-EMBS Special Topic Conference on Microtechnologies in Medicine and Biology. Proceedings (Cat. No. 02EX578), IEEE, Madison, WI, USA, 2002, pp. 261–264.
- 29 T. Stieglitz, H. Beutel, M. Schuettler and J.-U. Meyer, *Biomed. Microdevices*, 2000, **2**, 283–294.
- 30 V. P. Orlov, Y. A. Nashchekina, A. V. Nashchekin, O. N. Ozeryanskaya, S. D. Mirzametov and D. V. Svistov, *Pediatr. Traumatol. Orthop. Reconstr. Surg.*, 2022, **10**, 407–415.
- 31 D. Wu, X. Wang, Z. Wang and X. Wu, *J. Electrochem. Soc.*, 2023, **170**, 042505.
- 32 A. Bekmurzayeva, W. J. Duncanson, H. S. Azevedo and D. Kanayeva, *Mater. Sci. Eng., C*, 2018, **93**, 1073–1089.
- 33 M. Sarraf, E. Rezvani Ghomi, S. Alipour, S. Ramakrishna and N. Liana Sukiman, *Bio-Des. Manuf.*, 2022, **5**, 371–395.
- 34 R. D. Meyer, S. F. Cogan, T. H. Nguyen and R. D. Rauh, *IEEE Trans. Neural Syst. Rehabil. Eng.*, 2001, **9**, 2–11.
- 35 S. A. M. Marzouk, *Anal. Chem.*, 2003, **75**, 1258–1266.
- 36 H. R. Lim, N. Hillman, Y. T. Kwon, Y.-S. Kim, Y.-H. Choa and W.-H. Yeo, *Sens. Actuators, B*, 2020, **309**, 127761.
- 37 M. L. Hitchman and S. Ramanathan, *Analyst*, 1988, **113**, 35–39.
- 38 H. Suzuki, H. Arakawa, S. Sasaki and I. Karube, *Anal. Chem.*, 1999, **71**, 1737–1743.
- 39 E. Prats-Alfonso, L. Abad, N. Casañ-Pastor, J. Gonzalo-Ruiz and E. Baldrich, *Biosens. Bioelectron.*, 2013, **39**, 163–169.
- 40 C. Cheng, Y. Wu, X. Li, Z. An, Y. Lu, F. Zhang, B. Su and Q. Liu, *Sens. Actuators, B*, 2021, **349**, 130781.

- 41 M. Zea, A. Moya, M. Fritsch, E. Ramon, R. Villa and G. Gabriel, *ACS Appl. Mater. Interfaces*, 2019, **11**, 15160–15169.
- 42 A. Idili, J. Gerson, T. Kippin and K. W. Plaxco, *Anal. Chem.*, 2021, **93**, 4023–4032.
- 43 S. Li, J. Dai, M. Zhu, N. Arroyo-Currás, H. Li, Y. Wang, Q. Wang, X. Lou, T. E. Kippin, S. Wang, K. W. Plaxco, H. Li and F. Xia, *ACS Nano*, 2023, **17**, 18525–18538.
- 44 B. Gil, S. Anastasova and G.-Z. Yang, *Biosens. Bioelectron.*, 2021, **182**, 113175.
- 45 *Tietz fundamentals of clinical chemistry and molecular diagnostics*, ed. C. A. Burtis, D. E. Bruns, B. G. Sawyer and N. W. Tietz, Elsevier/Saunders, St. Louis, Missouri, 7th edn, 2015.
- 46 M. M. Patrick, J. M. Grillot, Z. M. Derden and D. W. Paul, *Electroanalysis*, 2017, **29**, 998–1005.
- 47 R. Trouillon, Z. Combs, B. A. Patel and D. O'Hare, *Electrochem. Commun.*, 2009, **11**, 1409–1413.
- 48 B. L. Hanssen, S. Siraj and D. K. Y. Wong, *Rev. Anal. Chem.*, 2016, **35**, 1–28.
- 49 U. N. Wijayarathna, S. D. Kiridena, J. D. Adams, C. J. Behrend and J. N. Anker, *Adv. Funct. Mater.*, 2021, **31**, 2104124.
- 50 I. Ges, B. Ivanov, D. Schaffer, E. Lima, A. Werdich and F. Baudenbacher, *Biosens. Bioelectron.*, 2005, **21**, 248–256.
- 51 S. Kakooei, M. C. Ismail and B. A. Wahjoedi, *Int. J. Electrochem. Sci.*, 2013, **8**, 3290–3301.
- 52 M. Veletić, E. H. Apu, M. Simić, J. Bergsland, I. Balasingham, C. H. Contag and N. Ashammakhi, *Chem. Rev.*, 2022, **122**, 16329–16363.
- 53 AO Fracture Monitor, <https://www.aofoundation.org/what-we-do/research-innovation/research-programs/projects/ao-fracture-monitor>, (accessed February 14, 2024).
- 54 P. Avaltroni, S. Nappi and G. Marrocco, *IEEE Sens. J.*, 2021, **21**, 21012–21021.